ACS OMEGA

http://pubs.acs.org/journal/acsodf

Article

Hydrogen-Bonded Organic Framework Structure: A Metal-Free Electrocatalyst for the Evolution of Hydrogen

Lopamudra Giri,* Bishnupad Mohanty, Ranjit Thapa, Bikash Kumar Jena,* and Venkateswara Rao Pedireddi

Cite This: *ACS Omega* 2022, 7, 22440−22446

Read Online

ACCESS | Metrics & More | Article Recommendations | Supporting Information

ABSTRACT: The hydrogen-bonded organic frameworks (HOFs) have gained significant attention due to their various alluring applications in the fascinating field of supramolecular chemistry. Herein, we report the electrocatalytic activity of HOFs toward the hydrogen evolution reaction (HER) by utilizing the molecular adduct of cyanuric and trithiocyanuric acid with various organic substrates (melamine and 4,4′-bipyridine). Both the experimental and theoretical findings provide insights and validate the electrocatalytic activity toward HER applications. This work contributes significantly to designing novel highly efficient metal-free HOF-based electrocatalysts for the HER.

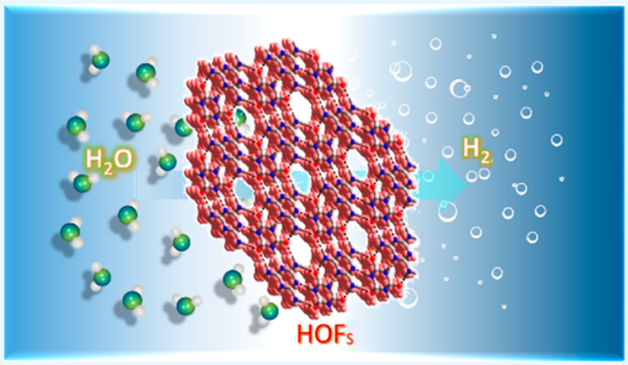

INTRODUCTION

Over the last decades, supramolecular chemistry has set a path toward a vibrant field of research due to its wider applications in the field of catalysis, organic synthesis, the chemistry of materials, medicine, and so forth.[1−4] In this endeavor, a myriad of new solids, composed of multimolecular components with elegant physical and chemical properties, have been intuitively designed via the molecular recognition process, utilizing various types of intermolecular interactions, for example, hydrogen bonds, which have been extensively reported in the literature.[5,6]

Hydrogen-bonded organic frameworks (HOFs) are porous crystalline materials constructed *via* intermolecular interactions formed by hydrogen atoms lying between two strongly electronegative atoms. The directional and flexible nature of hydrogen bonds allows for the design/reticulation of various framework structures such as covalent organic frameworks (COFs) and metal−organic frameworks (MOFs). In the last couple of years, varieties of functional HOFs have been synthesized and used for various potential applications such as separation,[7−10] sensing,[9,11,12] semiconductors,[8,10] gas adsorption,[13,14] supercapacitors,[15] catalysis,[16−21] and proton conductors.[22−24] Notably, Liu et al. synthesized bimetallic HOFs on nickel foam (HOF−Co_xFe_{1-x}) and studied the electrochemical water splitting.[25] Similarly, to create carbon-based oxygen reduction reaction (ORR) catalysts, Liu et al. used an HOF (HOF-8) as a precursor.[26] However, based on our knowledge, to date, there has been no report about metal-free HOF materials for electrochemical hydrogen evolution reaction (HER) applications.

Molecular hydrogen (H_2) is a promising candidate for future renewable energy sources due to its high efficiency, cleanliness, sustainability, and environmental friendliness.[27] Electrochemical water splitting is the most efficient method for hydrogen evolution.[19,22−24,28−30] Among a wide variety of electrocatalysts, Pt/C shows an unbeatable HER property. However, the low abundance, high cost, and poor stability of Pt seriously prohibit the development of the water electrolysis technology for commercial production of H_2.[17] Therefore, the fabrication of nonprecious electrocatalysts with low cost, high activity, and advanced stability is highly desirable. Thus, transition metal-based oxides,[18,19] sulfides,[22,23] phosphides,[24,31] nitrides,[32,33] carbides,[34] MOFs,[35,36,] and so forth have been well-tested for the desired catalytic activity, but these catalysts often suffer inherent corrosion and passivation in the acidic proton exchange membrane electrolyte.[37] Therefore, the possible development of metal-free HOF-based electrocatalysts for potential HER applications is profoundly essential. However, some high-quality research articles have been reported on the HER.[38−40] Nevertheless, exploring HOFs and their activity toward the HER provides a wide scope for the development of an alternate metal-free electrocatalyst of interest.

Received: March 16, 2022
Accepted: June 2, 2022
Published: June 21, 2022

https://doi.org/10.1021/acsomega.2c01585
ACS Omega 2022, 7, 22440−22446

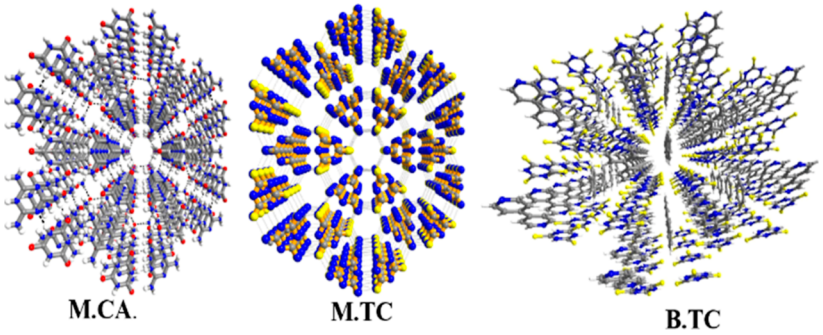

Figure 1. Scheme of the structure of the as-synthesized HOFs.

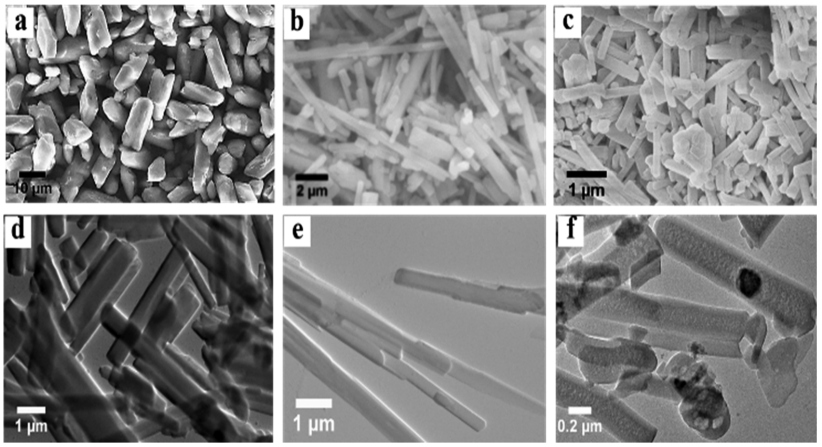

Figure 2. SEM (a−c) and TEM (d−f) images of the as-synthesized B.TC, M.TC, and M.CA, respectively.

EXPERIMENTAL SECTION

Chemicals and Reagents. All the chemicals have been purchased from Sigma-Aldrich with >99% purity and were used without additional purification.

Synthesis Procedure. Molecular adducts M.CA, M.TC, and B.TC were obtained via a facile one-step hydrothermal process by using the previously reported synthetic procedure (see the Supporting Information for the detailed description).

Powder X-ray Diffraction. Powder X-ray diffraction (PXRD) data were collected on a PANalytical diffractometer with Cu-Kα radiation (λ = 1.54060 Å). An X-ray generator with parameters of 40 kV and 30 mA was used to collect intensity data with a step size of 0.017° (2θ) in a continuous scanning mode. Diffraction patterns were collected in the 2θ range of 5−50° at room temperature.

Field Emission Scanning Electron Microscopy and Transmission Electron Microscopy Analysis. Field emission scanning electron microscopy (FESEM) images were obtained using a Carl Zeiss Merlin Compact instrument at an acceleration voltage of 5 kV. The transmission electron microscopy (TEM) images were obtained using an FEI-TECNIA G2 transmission electron microscope operating at 200 kV.

Electrochemical Measurement. All the measurements were performed in a three-compartment electrochemical cell on a CHI 760D electrochemical workstation at room temperature in a 0.5 M H_2SO_4 (pH = 0) solution for the HER. Linear sweep voltammetry (LSV) was performed at a scan rate of 5 mV/s. A glassy carbon electrode (GCE) was used as the working electrode. The GCE was prepolished using three different sizes of alumina powder in polishing cloth, sonicated with water for 10 min, and dried at room temperature. Ag/AgCl (3 M KCl) and Pt were used as reference electrodes and counter electrodes, respectively, in all measurements. All the polarization curves were transformed from the Ag/AgCl electrode to reversible hydrogen electrode (RHE) by using the formula $E_{RHE} = E_{Ag/AgCl} + 0.059\ pH\ E^0_{Ag/AgCl}$. The catalytic suspension was prepared by taking 1 mg of the as-synthesized sample dispersed in a mixed solution of 5 vol % Nafion and 95 vol % ethanol and sonicating for about 30 min into a homogeneous slurry. 5 μL of the slurry was deposited onto a polished GCE and dried in air. The mass loading of active materials was about 0.07 mg/cm^2. To evaluate the electrochemically active surface area (ECSA), cyclic voltammetry (CV) was carried out to probe the electrochemical double-layer capacitance (C_{dl}) of various samples at the non-Faradic region identified from CV. This non-Faradic region is typically a 0.1 V window about the open-circuit potential, and all measured current values are due to double-layer charging. A linear trend was observed by plotting the current at 0.15 V versus Ag/AgCl against the scan rate. The linear slope, equivalent to twice the double-layer capacitance C_{dl}, was used to present the ECSA. The measurement of the ECSA was performed according to eq 1.

$$ECSA = C_{dl}/C_s \quad (1)$$

where C_s is the specific capacitance of carbon-based compounds and the value of C_s is 27.5 μF/cm^2. The value of R_f can be calculated by dividing the electrode surface area (0.071 cm^2) by the ECSA values.

Computational Details. The theoretical calculations are performed using the spin-polarized density functional theory

https://doi.org/10.1021/acsomega.2c01585
ACS Omega 2022, 7, 22440−22446

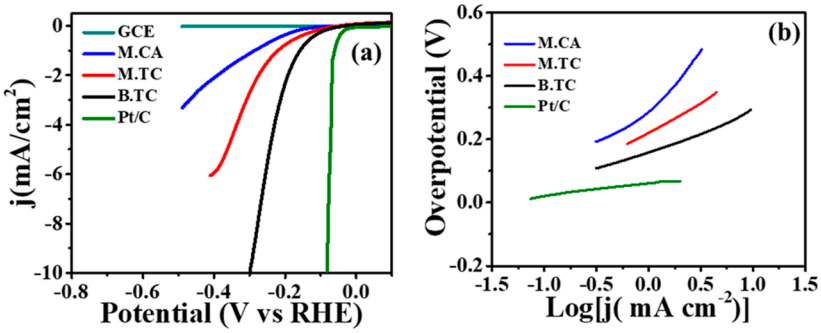

Figure 3. (a) HER polarization LSV plot of B.TC, M.TC, M.CA, and the GCE at a scan rate of 5 mV/s. (b) Corresponding Tafel plots.

(DFT), as implemented in the Vienna *ab initio* simulation package (VASP).[41] The potentials of the atoms are described using the projected augmented wave (PAW) method.[42] The generalized gradient approximation (GGA) is employed to consider the exchange and correlation effects at the Perdew–Burke–Ernzerhof (PBE) level.[43] A plane-wave cutoff energy of 450 eV is sufficient to obtain well-converged results. During relaxation, the Brillouin zone sampling is performed using a 5 × 5 × 1 Monkhorst–Pack grid. The maximum force converged to a value lower than 0.03 eV/Å, and the total energy converged to less than 10^{-6} eV per atom for obtaining the relaxed structures.

RESULTS AND DISCUSSION

In this work, we have synthesized three different hydrogen-bonded robust organic framework structures: M.CA, M.TC, and B.TC utilizing melamine (M), cyanuric acid (CA), trithiocyanuric acid (TC), and bipyridine (B) via simple hydrothermal methods.[44,45] The synthesis scheme for the three different structures is presented in the Supporting Information (Figure S1). Figure 1 presents the crystal structures of the as-synthesized materials under study. The as-synthesized B.TC, M.TC, and M.CA have been characterized using various techniques to ascertain their structure and morphology. The morphology of B.TC, M.TC, and M.CA complexes was investigated using FESEM and TEM measurements. Both the FESEM and TEM images confirmed that B.TC form a nano-leave-like morphology, whereas M.TC and M.CA show a nano-belt-like structure (Figure 2). The PXRD patterns verified the highly crystalline behavior of microcrystalline B.TC, M.TC, and M.CA (Figure S2). All the well-resolved peaks are in good agreement with the reported patterns.[44] For exploring the chemical stability of the complex, the synthesized materials were immersed in acidic, neutral, and alkaline conditions for about 24 h. After washing and drying, PXRD analysis was carried out, and the data show that all complexes retain their stability in acidic and neutral conditions. In contrast, all the complexes are unstable in alkaline conditions (Figure S3).

The as-synthesized HOF materials B.TC, M.TC, and M.CA were explored for the electrochemical generation of molecular hydrogen. All the catalysts were modified over the GCE with a mass loading of 0.70 mg/cm^2. The HER performance of B.TC, M.TC, and M.CA was examined along with that of the GCE for comparison. The LSV polarization curves were recorded in the Ar-saturated 0.5 M H_2SO_4 electrolyte at a 5 mV/s scan rate and are shown in Figure 3a. The increase in cathodic current density after a certain negative bias suggests HER initiation on the catalyst surface. In the case of M.CA, it catalyzes the HER at the onset overpotential of −0.13 V. However, upon replacing CA with TC, that is, for M.TC, the HER activity is enhanced, resulting in higher current density and a lower onset overpotential of −0.10 V. Similarly, upon replacing melamine (M) with bipyridine (B), that is, in the case of B.TC, further enhancement in the HER activity was observed compared to that of M.TC and M.CA. B.TC exhibits an onset potential of about −0.08 V, and after that, the cathodic current starts to increase, along with the simultaneous formations of gas bubbles on the electrode surface. A benchmark current density of 10 mA/cm^2 was achieved at the overpotential of −0.29 V. The obtained onset overpotential of catalyst B.TC is quite comparable with that of much earlier reported metal-free HER electrocatalysts. A comparison with previous reports was summarized and is presented in the Supporting Information (Table S1). However, it may be pertinent to mention that though B.TC possesses lower activity than the benchmark catalyst Pt/C, taking into account the cost and paucity of Pt, the efficacy of B.TC is appreciable toward the lower cost, metal-free, and facile synthesis process. The higher HER activity of B.TC may be accounted for by its interesting 3D channel-like structure, porous morphology, and HER active sites.

The Tafel slope is the intrinsic property of the materials, and it helps predict the mechanism and reaction kinetics for electrochemical reactions.[46,47] In the HER, the smaller Tafel slope of the catalysts suggests a faster proton reduction process at a lower potential. The Tafel slope is derived by fitting the linear part of the Tafel plot (η vs log j). In an acidic medium, the HER mechanism proceeds through three steps, that is, Volmer, Heyrovsky, and Tafel reactions: which is associated with the Tafel slopes of 120, 40, and 30 mV/dec, respectively. The Tafel slope for B.TC is nearly 78 mV/dec, which is much lower than that of M.TC (104 mV/dec) and M.CA (120 mV/dec) (Figure 3b) but higher than that of Pt/C (31 mV/dec). The Tafel slope for B.TC suggests that the Volmer–Heyrovsky mechanism is involved in the reaction process. The lower Tafel slope of B.TC indicates faster reaction kinetics toward the HER than that of M.TC and M.CA. Also, the magnitude of the current exchange density offers important information on the electrode performance. The exchange current density was evaluated from the Tafel plots using extrapolation methods (Figure S4). The B.TC electrocatalyst shows a higher exchange current density (j_o) of 0.047 mA/cm^2 than either M.TC (0.037 mA/cm^2) or M.CA (0.016 mA/cm^2). Further, it signifies the higher electrode kinetics and better activity of B.TC toward the HER. The electrochemical impedance spectroscopy measurement was carried out to study the electron transfer kinetics further. Catalyst B.TC shows a lower value of charge transfer resistance in the Nyquist plot than M.TC and M.CA (Figure

https://doi.org/10.1021/acsomega.2c01585
ACS Omega 2022, 7, 22440−22446

Table 1. Various Sites on the M.CA, M.TC, and B.TC Systems We Considered and the Overpotential of the Corresponding Systems During the HER

system (M.CA)	overpotential (η)	system (M.TC)	overpotential (η)	system (B.TC)	overpotential (η)
N-site-M-MCA	2.07	S-site-TC-M.TC	−1.22	C-site-TC-B.TC	1.601
C-site-M-MCA	2.47	C-site-TC-M.TC	−1.07	S-site-TC-B.TC	0.97
N-site-CA-MCA	2.43	C−S-site-M.TC	0.35	C−S-site-B.TC	0.2
C-site-CA-MCA	2.59				

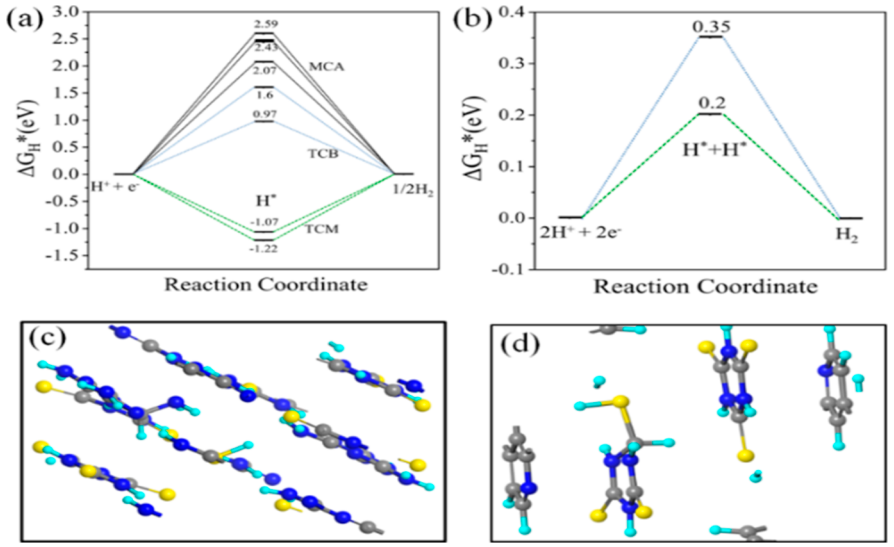

Figure 4. (a) Calculated free energy profile of the HER at the equilibrium potential for M.CA, M.TC, and B.TC complex structures. (b) Calculated free energy profile of the HER at the equilibrium potential for M.TC and B.TC structures considering the reaction of two hydrogen atoms at the same time. (c) 2H-adsorbed M.TC and (d) 2H-adsorbed B.TC structures. Dark blue, yellow, gray, and light blue colors denote the N, S, C, and H atoms, respectively.

S5). The better charge transfer resistance and higher metallic character in B.TC reflect the higher HER activity. Further, the electrochemical HER activity of materials is checked at different pH values of electrolytes. As the materials are unstable in an alkaline pH, the HER activity of B.TC, M.TC, and M.CA was explored in a neutral medium (1 M phosphate-buffered saline). As can be seen, all the electrocatalysts show a very poor HER activity in a neutral medium (Figure S6).

To obtain further insights into the HER activity, the DFT calculations have been performed to estimate the overpotential of the HER on the system considered in this work using the H* free energy profile. The HER activities of the three systems have been compared at the overpotential considering four possible sites of M.CA, three possible sites of M.TC, and three potential sites of B.TC.

The naming of the system is performed considering the type of active sites under study (Table 1). The free energy change during the formation of intermediate H* from the initial stage $H^+ + e^-$ is presented in Figure 4a. The Gibbs free energy of H* absorption ΔG_H* should be zero for an ideal catalyst. For the M.CA structure, the overpotential at each site is more than 2 eV, which is very high. The overpotential at the C site of TC of the M.TC complex is about −1.07 eV and that at the S site of TC of the B.TC structure is about 0.97 eV. The other values are demonstrated in Table 1. We can conclude that the presence of sulfur atoms increases the activity of the complex. To check the possibility of conversion of $2H + 2e^-$ on the complex at the same time, we consider the free energy profile of intermediate 2H* (Figure 4b). By considering this method, the overpotentials for the HER are calculated to be 0.35 and 0.2 eV on M.TC and B.TC structures, respectively, considering C and S as active sites (Figure 4c,d). This signifies that the sulfur atom and the structural arrangement are crucial for B.TC to be an efficient catalyst for the HER. The adsorption of 2H should be optimal to achieve lower overpotential.

In addition, the intrinsic catalytic activity and number of active sites of B.TC, M.TC, and M.CA were further verified by estimating the mass activity, specific activity, double-layer capacitance (C_{dl}), ECSA, roughness factor (R_f), and Faradaic efficiency. Catalyst B.TC exhibits the mass activity and specific activity values of 3.22 A/gm and 0.033 mA/cm^2, respectively, at the overpotential of 200 mV. The mass activity and specific activity of B.TC catalysts are much higher than those of M.TC and M.CA (Table S2).

The values of C_{dl}, ECSA, and R_f were directly proportional to the surface area of the catalyst and were used to estimate the number of active sites.[48] The detailed calculations of C_{dl}, ECSA, and R_f are presented in the Supporting Information. For the calculation of the C_{dl} value, the CV curve of each sample was recorded at the potential window from 0.1 to 0.2 V (vs Ag/AgCl) with different scan rates, as shown in Figure 5a−c. The current values from the anodic scan and cathodic scan at the middle potential (0.15 V) against the scan rates are plotted in Figure 5a′−c′. The linear slope is twice the C_{dl} value. The C_{dl} value of B.TC was calculated to be 35.5 μF, which is almost more than 2 times higher than that of M.TC (14 μF) and M.CA (11.5 μF). Similarly, the values of ECSA and R_f are summarized in Table S2. Thus, B.TC shows higher ECSA and R_f values as compared to M.TC and M.CA.

https://doi.org/10.1021/acsomega.2c01585
ACS Omega 2022, 7, 22440−22446

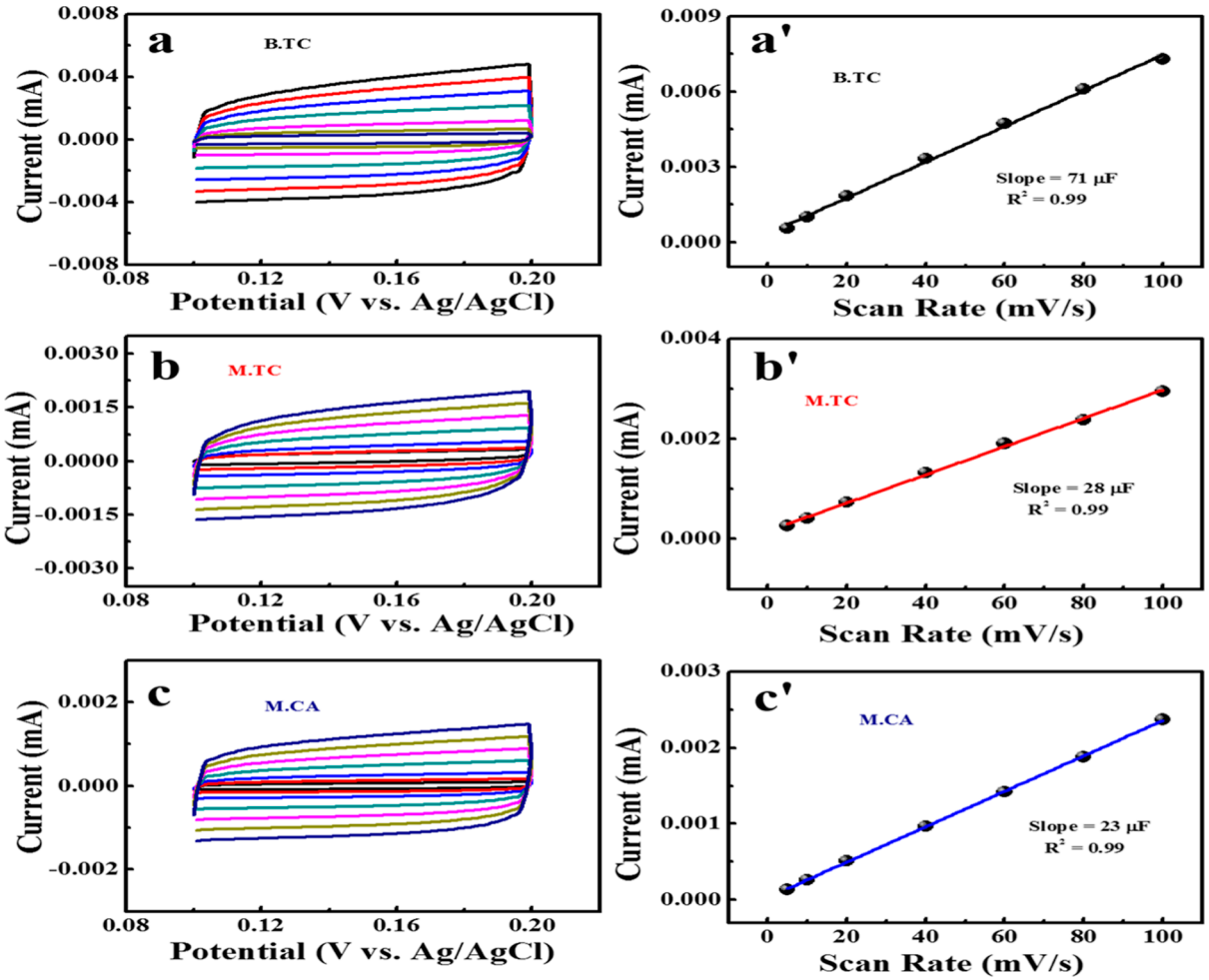

Figure 5. (a−c) Cyclic voltammograms obtained from the non-Faradic region of the as-synthesized B.TC, M.TC, and M.CA at different scan rates. (a′−c′) Corresponding plots of the scan rate vs the anodic current measured at 0.15 V.

The higher ECSA and R_f values of B.TC suggest that the enhanced HER activity might originate from the increased ECSA, thus exemplifying that B.TC has higher exposed catalytically active sites that significantly contribute to its excellent HER activity and establishing that the metal-free B.TC electrocatalyst holds a promising position in terms of higher activity toward the HER. The chemical stability and efficiency of a catalyst play a vital role in its practical application; thus, to address such points, a durability test is performed using the galvanostatic method at 5 mA/cm^2, as illustrated in Figure S7. Interestingly, it is observed that the current density was stable for 11 h, with more than 95% of the initial current being preserved, and the loss was negligible. After stability measurement, the study of the crystal structure is quite essential for electrocatalysts to validate the robust nature of the material. The PXRD analyses for sample B.TC have been carried out after 11 h of durability measurement. In the PXRD pattern, no predominant change in the crystal phase was observed, suggesting the stability of the crystalline HOF structure in the electrocatalyst (Figure S8). These results reflect its robustness for long-term reaction and justify its potential for promising application in various energy devices with alluring features.

CONCLUSIONS

In summary, the hydrogen-bonded porous organic framework structures of B.TC, M.TC, and M.CA significantly contribute to the HER in an acidic medium. B.TC possesses outstanding HER preference with a small overpotential of 80 mV, a Tafel slope of 78 mV/dec, an exchange current density of 0.047 mA/cm^2, and long-term durability. The overpotential values of experimental results are in good agreement with theoretical calculations. This novel material with a unique structure can be a good alternative metal-free electrocatalyst for energy devices.

ASSOCIATED CONTENT

Supporting Information

The Supporting Information is available free of charge at https://pubs.acs.org/doi/10.1021/acsomega.2c01585.

Experimental details; characterization; electrochemical measurement details; computational details and modeling; scheme of the synthesis procedures for B.TC, M.TC, and M.CA; PXRD pattern of the complexes: B.TC, M.TC, and M.CA; PXRD pattern showing the stability of the complex in different pH environments: B.TC, M.TC, and M.CA; exchange current density of B.TC, M.TC, and M.CA; Nyquist plot of B.TC, M.TC, and M.CA; chronopotentiometric measurement for the B.TC-modified electrode at a constant current density of

https://doi.org/10.1021/acsomega.2c01585
ACS Omega 2022, 7, 22440−22446

5 mA/cm^2; PXRD comparative study to determine the complexes' stability before and after the catalytic study; activity comparison of HOF compounds and reported metal-free materials toward the HER; and summarized electrochemical data of different as-synthesized electrocatalysts (PDF)

AUTHOR INFORMATION

Corresponding Authors

Lopamudra Giri − *CSIR-Institute of Minerals and Materials Technology, Bhubaneswar 751013 Odisha, India; Solid State and Supramolecular Structural Chemistry Laboratory, School of Basic Sciences, Indian Institute of Technology Bhubaneswar, Bhubaneswar 752 050, India*; Email: lg10@iitbbs.ac.in

Bikash Kumar Jena − *CSIR-Institute of Minerals and Materials Technology, Bhubaneswar 751013 Odisha, India; Academy of Scientific & Innovative Research, Ghaziabad 201002, India*; orcid.org/0000-0003-1794-4430; Email: bikash@immt.res.in

Authors

Bishnupad Mohanty − *CSIR-Institute of Minerals and Materials Technology, Bhubaneswar 751013 Odisha, India*; orcid.org/0000-0001-7320-1223

Ranjit Thapa − *Department of Physics, SRM University—AP, Amaravati 52240 Andhra Pradesh, India*; orcid.org/0000-0002-9285-0525

Venkateswara Rao Pedireddi − *Solid State and Supramolecular Structural Chemistry Laboratory, School of Basic Sciences, Indian Institute of Technology Bhubaneswar, Bhubaneswar 752 050, India*

Complete contact information is available at: https://pubs.acs.org/10.1021/acsomega.2c01585

Notes

The authors declare no competing financial interest.

ACKNOWLEDGMENTS

B.K.J. thanks the director of CSIR-IMMT for his kind permission and encouragement in completing this work. BPM is grateful to UGC, India, for the fellowship. B.K.J. acknowledges UGC, CSR, India, BRNS, Mumbai, India (No-2013/37P/67/BRNS); MNRE, New Delhi, India (No-102/87/2011-NT); and CSIR (H2T program, HCP-44 FBR1.2), New Delhi, India HRDG YSP-02 (P-81−113) for the financial support. L.G. and V.R.P. thank the MoE for their financial support. The authors thank Prof. P. V. Satyam for helping with the TEM analysis. R.T. thanks the SRM Supercomputer Center of SRM Institute of Science and Technology for providing the computational facility.

REFERENCES

(1) Chin, D. N.; Gordon, D. M.; Whitesides, G. M. Computational Simulations of Supramolecular Hydrogen-Bonded Aggregates: HubM3, FlexM3, and Adamantane-Based Hubs in Chloroform. *J. Am. Chem. Soc.* **1994**, *116*, 12033−12044.

(2) Raynal, M.; Ballester, P.; Vidal-Ferran, A.; van Leeuwen, P. W. N. M. Supramolecular Catalysis. Part 2: Artificial Enzyme Mimics. *Chem. Soc. Rev.* **2014**, *43*, 1734−1787.

(3) Desiraju, G. R. Chemistry beyond the Molecule. *Nature* **2001**, *412*, 397−400.

(4) Astruc, D.; Boisselier, E.; Ornelas, C. Dendrimers Designed for Functions: From Physical, Photophysical, and Supramolecular Properties to Applications in Sensing, Catalysis, Molecular Electronics, Photonics, and Nanomedicine. *Chem. Rev.* **2010**, *110*, 1857−1959.

(5) Minch, M. J. An Introduction to Hydrogen Bonding (Jeffrey, George A.). *J. Chem. Educ.* **1999**, *76*, 759.

(6) Przybysz, P.; Dubowik, M.; Kucner, M. A.; Przybysz, K.; Przybysz Buzała, K. Contribution of Hydrogen Bonds to Paper Strength Properties. *PLoS One* **2016**, *11*, No. e0155809.

(7) Li, P.; He, Y.; Zhao, Y.; Weng, L.; Wang, H.; Krishna, R.; Wu, H.; Zhou, W.; O'Keeffe, M.; Han, Y.; Chen, B. A Rod-Packing Microporous Hydrogen-Bonded Organic Framework for Highly Selective Separation of C2H2/CO2 at Room Temperature. *Angew. Chem., Int. Ed.* **2014**, *54*, 574−577.

(8) Liu, X.; Yang, X.; Wang, H.; Hisaki, I.; Wang, K.; Jiang, J. A Robust Redox-Active Hydrogen-Bonded Organic Framework for Rechargeable Batteries. *J. Mater. Chem. A* **2022**, *10*, 1808.

(9) Wang, H.; Bao, Z.; Wu, H.; Lin, R.-B.; Zhou, W.; Hu, T.-L.; Li, B.; Zhao, J. C.-G.; Chen, B. Two Solvent-Induced Porous Hydrogen-Bonded Organic Frameworks: Solvent Effects on Structures and Functionalities. *Chem. Commun.* **2017**, *53*, 11150−11153.

(10) Dalapati, S.; Saha, R.; Jana, S.; Patra, A. K.; Bhaumik, A.; Kumar, S.; Guchhait, N. A Multifunctional Porous Organic Schottky Barrier Diode. *Angew. Chem., Int. Ed.* **2012**, *51*, 12534−12537.

(11) Liu, Y.; Xu, X.; Lu, H.; Yan, B. Dual-Emission Ratiometric Fluorescent Probe-Based Lanthanide-Functionalized Hydrogen-Bonded Organic Framework for the Visual Detection of Methylamine. *J. Mater. Chem. C* **2022**, *10*, 1212.

(12) Feng, J.-f.; Yan, X.-Y.; Ji, Z.-Y.; Liu, T.-F.; Cao, R. Fabrication of Lanthanide-Functionalized Hydrogen-Bonded Organic Framework Films for Ratiometric Temperature Sensing by Electrophoretic Deposition. *ACS Appl. Mater. Interfaces* **2020**, *12*, 29854−29860.

(13) Luo, X.-Z.; Jia, X.-J.; Deng, J.-H.; Zhong, J.-L.; Liu, H.-J.; Wang, K.-J.; Zhong, D.-C. A Microporous Hydrogen-Bonded Organic Framework: Exceptional Stability and Highly Selective Adsorption of Gas and Liquid. *J. Am. Chem. Soc.* **2013**, *135*, 11684−11687.

(14) Wang, J.-X.; Pei, J.; Gu, X.-W.; Lin, Y.-X.; Li, B.; Qian, G. Efficient CO2/CO Separation in a Stable Microporous Hydrogen-Bonded Organic Framework. *Chem. Commun.* **2021**, *57*, 10051−10054.

(15) Halder, A.; Ghosh, M.; Khayum M, A.; Bera, S.; Addicoat, M.; Sasmal, H. S.; Karak, S.; Kurungot, S.; Banerjee, R. Interlayer Hydrogen-Bonded Covalent Organic Frameworks as High-Performance Supercapacitors. *J. Am. Chem. Soc.* **2018**, *140*, 10941−10945.

(16) Voiry, D.; Fullon, R.; Yang, J.; de Carvalho Castro e Silva, C.; Kappera, R.; Bozkurt, I.; Kaplan, D.; Lagos, M. J.; Batson, P. E.; Gupta, G.; Mohite, A. D.; Dong, L.; Er, D.; Shenoy, V. B.; Asefa, T.; Chhowalla, M. The Role of Electronic Coupling between Substrate and 2D MoS2 Nanosheets in Electrocatalytic Production of Hydrogen. *Nat. Mater.* **2016**, *15*, 1003−1009.

(17) Bhanja, P.; Mohanty, B.; Patra, A. K.; Ghosh, S.; Jena, B. K.; Bhaumik, A. IrO2 and Pt Doped Mesoporous SnO2 Nanospheres as Efficient Electrocatalysts for the Facile OER and HER. *ChemCatChem* **2019**, *11*, 583−592.

(18) Jin, Y.; Wang, H.; Li, J.; Yue, X.; Han, Y.; Shen, P. K.; Cui, Y. Porous MoO2Nanosheets as Non-Noble Bifunctional Electrocatalysts for Overall Water Splitting. *Adv. Mater.* **2016**, *28*, 3785−3790.

(19) Dalai, N.; Mohanty, B.; Mitra, A.; Jena, B. Highly Active Ternary Nickel−Iron Oxide as Bifunctional Catalyst for Electrochemical Water Splitting. *ChemistrySelect* **2019**, *4*, 7791−7796.

(20) Zhang, N.; Yin, Q.; Guo, S.; Chen, K.-K.; Liu, T.-F.; Wang, P.; Zhang, Z.-M.; Lu, T.-B. Hot-Electron Leading-out Strategy for Constructing Photostable HOF Catalysts with Outstanding H2 Evolution Activity. *Appl. Catal., B* **2021**, *296*, 120337.

(21) Han, B.; Wang, H.; Wang, C.; Wu, H.; Zhou, W.; Chen, B.; Jiang, J. Postsynthetic Metalation of a Robust Hydrogen-Bonded Organic Framework for Heterogeneous Catalysis. *J. Am. Chem. Soc.* **2019**, *141*, 8737−8740.

(22) Fu, W.; He, H.; Zhang, Z.; Wu, C.; Wang, X.; Wang, H.; Zeng, Q.; Sun, L.; Wang, X.; Zhou, J.; Fu, Q.; Yu, P.; Shen, Z.; Jin, C.; Yakobson, B. I.; Liu, Z. Strong Interfacial Coupling of MoS2/g-C3N4 van de Waals Solids for Highly Active Water Reduction. *Nano Energy* **2016**, *27*, 44−50.
(23) Kamila, S.; Mohanty, B.; Samantara, A. K.; Guha, P.; Ghosh, A.; Jena, B.; Satyam, P. V.; Mishra, B. K.; Jena, B. K. Highly Active 2D Layered MoS 2 -RGO Hybrids for Energy Conversion and Storage Applications. *Sci. Rep.* **2017**, *7*, 8378.
(24) Shi, Y.; Zhang, B. Recent Advances in Transition Metal Phosphide Nanomaterials: Synthesis and Applications in Hydrogen Evolution Reaction. *Chem. Soc. Rev.* **2016**, *45*, 1529−1541.
(25) Liu, F. Q.; Liu, J. W.; Gao, Z.; Wang, L.; Fu, X.-Z.; Yang, L. X.; Tao, Y.; Yin, W. H.; Luo, F. Constructing Bimetal-Complex Based Hydrogen-Bonded Framework for Highly Efficient Electrocatalytic Water Splitting. *Appl. Catal., B* **2019**, *258*, 117973.
(26) Liu, W.-J.; Wen, Y.-Q.; Wang, J.-W.; Zhong, D.-C.; Tan, J.-B.; Lu, T.-B. Nitrogen- and Iodine-Doped Microporous Carbon Derived from a Hydrogen-Bonded Organic Framework: An Efficient Metal-Free Electrocatalyst for the Oxygen Reduction Reaction. *J. Mater. Chem. A* **2019**, *7*, 9587−9592.
(27) Cook, T. R.; Dogutan, D. K.; Reece, S. Y.; Surendranath, Y.; Teets, T. S.; Nocera, D. G. Solar Energy Supply and Storage for the Legacy and Nonlegacy Worlds. *Chem. Rev.* **2010**, *110*, 6474−6502.
(28) Mohanty, B.; Bhanja, P.; Jena, B. K. An Overview on Advances in Design and Development of Materials for Electrochemical Generation of Hydrogen and Oxygen. *Mater. Today Energy* **2022**, *23*, 100902.
(29) Mohanty, B.; Mitra, A.; Jena, B.; Jena, B. K. MoS2 Quantum Dots as Efficient Electrocatalyst for Hydrogen Evolution Reaction over a Wide PH Range. *Energy Fuels* **2020**, *34*, 10268−10275.
(30) Ruidas, S.; Mohanty, B.; Bhanja, P.; Erakulan, E. S.; Thapa, R.; Das, P.; Chowdhury, A.; Mandal, S. K.; Jena, B. K.; Bhaumik, A. Metal-Free Triazine-Based 2D Covalent Organic Framework for Efficient H2 Evolution by Electrochemical Water Splitting. *ChemSusChem* **2021**, *14*, 5057−5064.
(31) Dutta, A.; Samantara, A. K.; Dutta, S. K.; Jena, B. K.; Pradhan, N. Surface-Oxidized Dicobalt Phosphide Nanoneedles as a Nonprecious, Durable, and Efficient OER Catalyst. *ACS Energy Lett.* **2016**, *1*, 169−174.
(32) Xie, J.; Li, S.; Zhang, X.; Zhang, J.; Wang, R.; Zhang, H.; Pan, B.; Xie, Y. Atomically-Thin Molybdenum Nitride Nanosheets with Exposed Active Surface Sites for Efficient Hydrogen Evolution. *Chem. Sci.* **2014**, *5*, 4615−4620.
(33) Wang, Y.; Xie, C.; Liu, D.; Huang, X.; Huo, J.; Wang, S. Nanoparticle-Stacked Porous Nickel−Iron Nitride Nanosheet: A Highly Efficient Bifunctional Electrocatalyst for Overall Water Splitting. *ACS Appl. Mater. Interfaces* **2016**, *8*, 18652−18657.
(34) Li, J.-S.; Wang, Y.; Liu, C.-H.; Li, S.-L.; Wang, Y.-G.; Dong, L.-Z.; Dai, Z.-H.; Li, Y.-F.; Lan, Y.-Q. Coupled Molybdenum Carbide and Reduced Graphene Oxide Electrocatalysts for Efficient Hydrogen Evolution. *Nat. Commun.* **2016**, *7*, 11204.
(35) Pal, S.; Sahoo, M.; Veettil, V. T.; Tadi, K. K.; Ghosh, A.; Satyam, P.; Biroju, R. K.; Ajayan, P. M.; Nayak, S. K.; Narayanan, T. N. Covalently Connected Carbon Nanotubes as Electrocatalysts for Hydrogen Evolution Reaction through Band Engineering. *ACS Catal.* **2017**, *7*, 2676−2684.
(36) Aiyappa, H. B.; Thote, J.; Shinde, D. B.; Banerjee, R.; Kurungot, S. Cobalt-Modified Covalent Organic Framework as a Robust Water Oxidation Electrocatalyst. *Chem. Mater.* **2016**, *28*, 4375−4379.
(37) Popczun, E. J.; McKone, J. R.; Read, C. G.; Biacchi, A. J.; Wiltrout, A. M.; Lewis, N. S.; Schaak, R. E. Nanostructured Nickel Phosphide as an Electrocatalyst for the Hydrogen Evolution Reaction. *J. Am. Chem. Soc.* **2013**, *135*, 9267−9270.
(38) Hu, C.; Liu, D.; Xiao, Y.; Dai, L. Functionalization of Graphene Materials by Heteroatom-Doping for Energy Conversion and Storage. *Prog. Nat. Sci.: Mater. Int.* **2018**, *28*, 121−132.
(39) Jiao, Y.; Zheng, Y.; Davey, K.; Qiao, S.-Z. Activity Origin and Catalyst Design Principles for Electrocatalytic Hydrogen Evolution on Heteroatom-Doped Graphene. *Nat. Energy* **2016**, *1*, 16130.
(40) Patra, B. C.; Khilari, S.; Manna, R. N.; Mondal, S.; Pradhan, D.; Pradhan, A.; Bhaumik, A. A Metal-Free Covalent Organic Polymer for Electrocatalytic Hydrogen Evolution. *ACS Catal.* **2017**, *7*, 6120−6127.
(41) Kresse, G.; Furthmüller, J. Efficiency of Ab-Initio Total Energy Calculations for Metals and Semiconductors Using a Plane-Wave Basis Set. *Comput. Mater. Sci.* **1996**, *6*, 15−50.
(42) Dal Corso, A. Projector Augmented-Wave Method: Application to Relativistic Spin-Density Functional Theory. *Phys. Rev. B: Condens. Matter Mater. Phys.* **2010**, *82*, 75116.
(43) Perdew, J. P.; Burke, K.; Ernzerhof, M. Generalized Gradient Approximation Made Simple. *Phys. Rev. Lett.* **1996**, *77*, 3865−3868.
(44) Ranganathan, A.; Pedireddi, V. R.; Chatterjee, S.; Rao, C. N. R. An Organic Channel Structure Formed by the Supramolecular Assembly of Trithiocyanuric Acid and 4,4′-Bipyridyl. *J. Mater. Chem.* **1999**, *9*, 2407−2411.
(45) Ranganathan, A.; Pedireddi, V. R.; Rao, C. N. R. Hydrothermal Synthesis of Organic Channel Structures: 1:1 Hydrogen-Bonded Adducts of Melamine with Cyanuric and Trithiocyanuric Acids. *J. Am. Chem. Soc.* **1999**, *121*, 1752−1753.
(46) Mondal, S.; Mohanty, B.; Nurhuda, M.; Dalapati, S.; Jana, R.; Addicoat, M.; Datta, A.; Jena, B. K.; Bhaumik, A. A Thiadiazole-Based Covalent Organic Framework: A Metal-Free Electrocatalyst toward Oxygen Evolution Reaction. *ACS Catal.* **2020**, *10*, 5623−5630.
(47) Mohanty, B.; Wei, Y.; Ghorbani-Asl, M.; Krasheninnikov, A. V.; Rajput, P.; Jena, B. K. Revealing the Defect-Dominated Oxygen Evolution Activity of Hematene. *J. Mater. Chem. A* **2020**, *8*, 6709.
(48) Mohanty, B.; Ghorbani-Asl, M.; Kretschmer, S.; Ghosh, A.; Guha, P.; Panda, S. K.; Jena, B.; Krasheninnikov, A. V.; Jena, B. K. MoS2 Quantum Dots as Efficient Catalyst Materials for the Oxygen Evolution Reaction. *ACS Catal.* **2018**, *8*, 1683−1689.

https://doi.org/10.1021/acsomega.2c01585
ACS Omega 2022, 7, 22440−22446